Modelling and characterization of nonlinear mechanical behaviour of perfect and imperfect gamma-graphyne

Filipe Cabaça Rodrigues
filipe.c.rodrigues@tecnico.ulisboa.pt

Instituto Superior Técnico, Lisboa, Portugal

November 2016

Abstract

γ-Graphyne is a carbon allotrope with two-dimensional geometry, whose molecular structure is composed of *sp* and sp^2 hybridized carbon atoms, comprising aromatic hexagonal rings and acetylenic groups. Based on its structure and excellent mechanical, electronic and optical properties, this nanomaterial shows several promising applications. The main objective of this thesis is the development of a consistent finite element model for the simulation of the nonlinear mechanical behaviour of both perfect and imperfect γ-graphyne. The linear and non linear elastic mechanical properties of the perfect γ-graphyne were evaluated for tensile and compressive directions, using three interatomic potentials to describe the present interactions in the structure. The computational analysis of the defective sheets intended to evaluate the influence of vacancy defects on the linear and nonlinear mechanical properties of γ-graphyne. The results obtained were then compared with results reported in the literature from previous investigations using molecular dynamics and other atomistic methods. This validation shows that the developed finite element model is able to predict correctly the linear and nonlinear mechanical properties of γ-graphyne with and without defects.
Keywords: γ-Graphyne, Nanomaterials, Vacancy Defects, Mechanical Properties, Nonlinear Behaviour

1. Introduction

Carbon has various hybridized states (*sp*, sp^2 and sp^3), which enable it to bind to itself and with other elements. Diamond and graphite are the most known crystalline forms of this element, but it also has numerous allotropes, like graphene, carbon nanotubes (CNTs) or the different forms of graphyne [14]. Carbon-based nanomaterials have attracted the interest of researchers in the last few years due to their unique mechanical, electrical, thermal and optical properties [7], allowing the application of these properties in various engineering fields. For example, graphene and CNTs can be used to increase the stiffness and strength of structural composites and decreasing their weight [4] and thermal expansion coefficient [22] in the aerospace sector. In electronics, CNTs could replace copper on an airplane's wires, turning them lighter and more efficient [15], while graphene and graphyne show promising applications in high-ratio transistors, energy storage and sensors, which could be used to improve electronic systems [20].

γ-Graphyne is a two-dimensional carbon allotrope whose molecular structure is composed of *sp* and sp^2 hybridized carbon atoms, comprising aromatic hexagonal rings and acetylenic groups as can be seen in figure 1. The first molecular segments of this nanomaterial were first synthesized by *Haley* [13] in 2008, but since then there have been no reports of large sheets synthesis [9]. Multiple efforts have been made to develop computational models capable of predicting the mechanical behaviour of γ-graphyne. Cranford and Buehler [9] used Molecular Dynamics (MD) in order to simulate this behaviour, predicting the Young modulus (533 and 700 $[GPa]$) and the ultimate stresses (48 and 108 $[GPa]$) for both tested directions. Using Density Functional Theory (DFT) calculations, Peng *et al.* [21] predicted the in-plane Young modulus to be 162 $[N/m]$ and the ultimate stresses (56 and 59 $[GPa]$) for both tested directions.

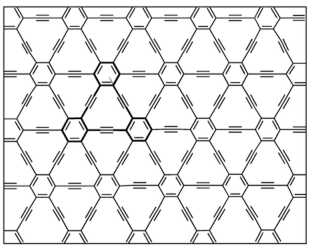

Figure 1: Scheme of the structure of γ-graphyne [13]

The mentioned methods, MD and DFT, require a great amount of computational effort and time investment. This work proposes a model based on the Finite Element Method (FEM) to study the nonlinear mechanical behaviour of γ-graphyne, based on the atomistic equivalent-continuum method first provided by Odegard *et al.* [18]. Although this approach has been used to simulate the mechanical behaviour of graphene and CNTs, there is only a single article about γ-graphyne's mechanical elastic properties using FEM, written by Couto [8].

2. Background

2.1. Molecular mechanics (MM)

In MM, the atomic structure is treated as a system of multiple particles interacting with neighbouring particles. The total interatomic potential energy U_{total} of a nano-structured system is then given by the sum of different energy contributions, as suggested by the following equation:

$$U_{total} = \sum(U_r + U_\theta + U_\phi + U_\omega) + \sum U_{vdw}\,, \quad (1)$$

where the first four terms represent the potential energy of the interactions between bonded atoms, more precisely the stretching U_r and the angle bending U_θ bonds, and the in-plane U_ϕ and out-plane U_ω torsion terms. The last term U_{vdw} corresponds to the potential energy of the van der Waals (vdW) interactions between non-bonded atoms.

All the mentioned potentials can be described by interatomic potentials. The Morse potential [17] has been widely used to describe the U_r and U_θ potentials for $C-C$ bonds, while the 6-12 Lennard-Jones (L-J) potential [16] is commonly used for the U_{vdw}. The next three equations present U_r, U_θ and U_{vdW} mentioned potentials, respectively.

$$U_r = D_e([1 - e^{-\beta(r-r_0)}]^2 - 1). \quad (2)$$

$$U_\theta = \frac{1}{2}k_\theta(\theta - \theta_0)^2[1 + k_6(\theta - \theta_0)^4]. \quad (3)$$

$$U_{vdw}(r) = 4D\left(\frac{d^{12}}{r^{12}} - \frac{d^6}{r^6}\right). \quad (4)$$

The present terms in these equations will be discussed in section 3.

3. Implementation

This thesis intends to simulate the nonlinear mechanical behaviour of a γ-graphyne sheet. Using the finite element software *ANSYS® 16*, the various interactions present on the structure of the material were modelled using nonlinear (*COMBIN39*) and linear (*COMBIN14*) spring elements. In order to apply the potentials mentioned in section 2, the corresponding force per displacement curves has to be obtained. In the next three subsections, this process will be described regarding all the bonds that were taken into account in the developed model.

3.1. Stretching forces

The structure of γ-graphyne is composed by three types of covalent bonds: single $(C-C)$, aromatic $(C=C)$ and triple $(C\equiv C)$, as illustrated on figure 2.

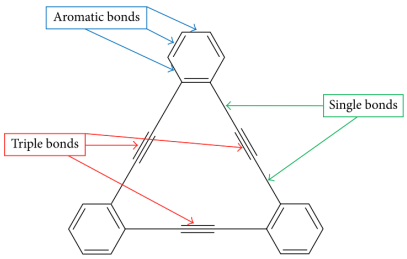

Figure 2: Covalent bonds of γ-graphyne [8]

To simulate the mechanical behaviour of each bond type, the corresponding F vs. Δr curves must be determined. The following expression is obtained by deriving the Morse potential equation 2:

$$F(\Delta r) = \frac{\partial(U_r)}{\partial(\Delta r)} = 2D_e\beta(1-e^{-\beta(\Delta r)})e^{-\beta(\Delta r)}, \quad (5)$$

where $\Delta r = r - r_0$ represents the axial deformation of the covalent bond length, D_e corresponds to the dissociation energy and β is a parameter to control the potential. The values from Peng *et al.* [21] article for the three covalent bonds were used for the initial bond lengths r_0. For the single bond, the β and D_e values could be found in an article by Belytschko *et al.* [5]. For the aromatic and the triple bonds, the D_e values were found in a paper written by Blanksby [6]. The β parameter for these two bond types were not available in the literature, so the values were linearly extrapolated from the ones corresponding to the single bonds. All the reported data are presented in table 3.1.

Table 1: Values for r_0, D_e and β

Bond Type	r_0 $[nm]$	D_e $[N.m]$	β $[m^{-1}]$
$C-C$	$0,1407$	$6,03{\cdot}10^{-19}$	$2,63{\cdot}10^{10}$
$C=C$	$0,1426$	$1,03{\cdot}10^{-18}$	$4,49{\cdot}10^{10}$
$C\equiv C$	$0,1223$	$1,39{\cdot}10^{-18}$	$6,05{\cdot}10^{10}$

Using the data present in table 3.1, it was then possible to determine the F vs. Δr curves corresponding to the three covalent bond types. The acetylenic linkage consists in a series of single-triple-single (S-T-S) bonds. To obtain the behaviour of the three bonds simultaneously with the objective of replacing the three individual springs by just one in the model, this linkage was simulated with FEM and the respective F vs. Δr curve of the series

was calculated. The four obtained curves are represented in the graphic of figure 3.

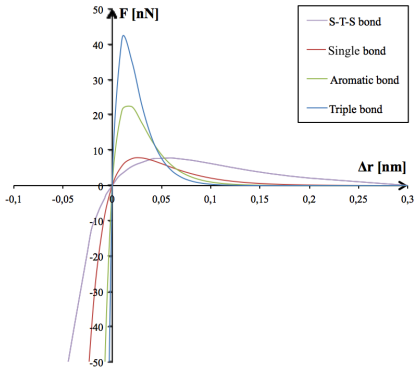

Figure 3: F vs. Δr curves for the stretching bonds

3.2. Angle bending forces

The angle bending forces were also taken into account on the aromatic benzenic rings. To obtain the respective force field, the derivative form of the corresponding Morse potential for the angle bending bonds (see equation 3) must be determined [23], assuming small angular bond changes $\Delta\theta = (2\Delta R)/r_0$ [18]:

$$F(\Delta R) = \frac{4}{r_0^2} k_\theta (R - R_0)\left[1 + \frac{48}{r_0^2} k_6 (R - R_0)^4\right], \quad (6)$$

where $R_0 = 0,247[nm]$ is the initial angle bending element length and r_0 is the initial aromatic covalent bond length. The values used for the parameters k_θ and k_6 are $0,9$ $[\frac{nNnm}{rad^2}]$ and $0,754$ $[rad^{-4}]$ [5], respectively. In figures 4 a) and b), the F vs. ΔR curve obtained from the equation 6 and a scheme with the angle bending bonds application on a benzenic aromatic ring are presented.

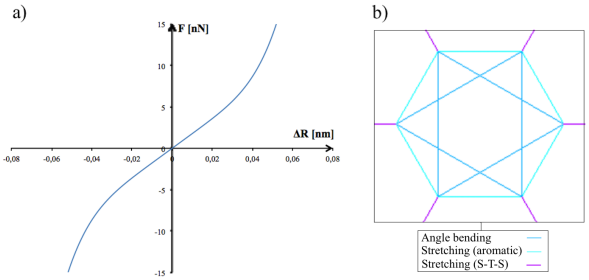

Figure 4: a) F vs. Δr curves for the angle bending bonds; b) Aromatic ring scheme with the stretching and angle bending bonds represented

3.3. van der Waals forces

The interactions of non-bonded carbon atoms can be described by the vdW forces. The derivative form of the 6-12 L-J potential, equation 4, gives the vdW force field, as demonstrated in the next expression:

$$F_{vdw}(r) = \frac{24D}{d}\left(2\left(\frac{d}{r}\right)^{13} - \left(\frac{d}{r}\right)^{7}\right), \quad (7)$$

where r is the actual distance between the two non-bonded atoms, D corresponds to the bond energy and d is a constant that corresponds to the equilibrium atomic distance. For two carbon atoms, D_{ij} and d_{ij} take the values of $4,862{\cdot}10^{-4}$ $[nN.nm]$ and $0,355[nm]$ [19], respectively.

Due to the fact that these interactions are significantly weaker [11] than the stretching or the angle bending ones, it was decided to simplify the model and use them as linear springs. From the equation 7, it was possible to calculate the vdW spring constant k_{vdw}, as shown bellow.

$$k_{vdw} = \left.\frac{\partial(F_{vdw}(r))}{\partial(r)}\right|_{r=d} = 1,76\left[\frac{nN}{nm}\right]. \quad (8)$$

The scheme present in figure 5 shows a detailed molecular segment of γ-graphyne with the respective vdW spring elements represented, as well as the stretching ones.

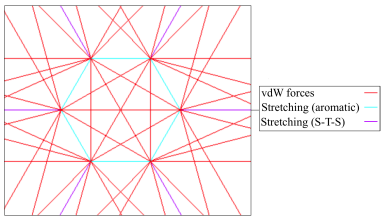

Figure 5: Aromatic ring scheme with the stretching bonds and vdW forces represented

3.4. Geometric modelling of the finite element mesh

In order to use the force fields described in the last subsections, the γ-graphyne sheet model was then built. Using the finite element (FE) software *ANSYS® 16*, a simple γ-graphyne molecule was first modelled using lines. After that, using mirroring commands, it was possible to obtain a complete sheet with the dimensions $10,9[nm]$ (L_i) and $9,8[nm]$ (H_i) in the armchair (x) and zig-zag (y) directions, respectively. To finish the model the mesh was then made, associating the multiple lines to the respective spring type by applying the force fields described before. The final γ-graphyne sheet nonlinear spring model is presented in figure 6.

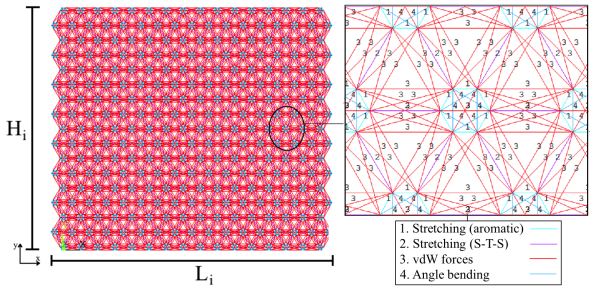

Figure 6: γ-Graphyne sheet final FE model

3.5. Analysis and boundary conditions

Using the sheet model presented in subsection 3.4, several analyses can be done to characterize the mechanical behaviour of γ-graphyne. The adopted simulations are:

- Uniaxial tension and compression tests in the armchair (x) direction, with the purpose of acquiring the linear elastic (Young modulus E_x and Poisson coefficient ν_{yx}) and non linear elastic (ultimate stress $\sigma_{u,x}$ and strain $\epsilon_{u,x}$) properties.
- Uniaxial tension and compression tests in the zig-zag (y) direction, with the purpose of acquiring the linear elastic (Young modulus E_y and Poisson coefficient ν_{xy}) and non linear elastic (ultimate stress $\sigma_{u,y}$ and strain $\epsilon_{u,y}$) properties.
- Biaxial tension and compression tests (xy plane), in order to acquire the linear elastic (bulk modulus K_{xy}) and non linear elastic (ultimate average stress $\overline{\sigma}_u$ and respective variation on the sheet's section area ΔA_u) properties.
- Shear test (xy plane), with the purpose of obtaining the shear modulus (G_{xy}), and the ultimate shear stress τ_{xy} and angle γ.

For all the mentioned analyses, displacements were applied in the desired nodes. For each type of analysis, some nodes were also constrained in order to prevent the rigid body move and to get the corresponding reaction forces of the nodes. These data are necessary to obtain the mechanical properties of γ-graphyne.

4. Results

4.1. Results presentation

For the evaluation of the γ-graphyne's mechanical properties, nonlinear simulations were made using the FE software *ANSYS® 16*, which uses the Newton-Raphson iterative method to get the converged solutions. In the next figure, four undeformed and deformed γ-graphyne sheet configurations are presented, corresponding to the last steps of the obtained nonlinear solutions for the tension cases of the analysis described in subsection 3.5. Figures 8 a) and b) correspond to the uniaxial analyses in x and y direction, respectively, while figures 8 c) and d) correspond, respectively, to the biaxial and shear analysis. In order to give a clearer perception to the reader, the springs that simulate the angle bending and vdW forces were visually omitted.

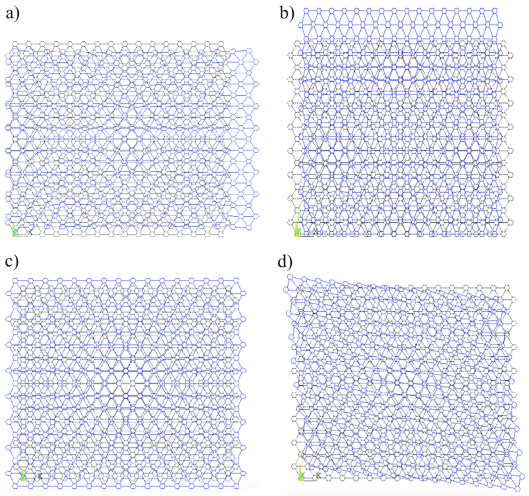

Figure 7: a-d) Deformed and undeformed sheet's configurations for the considered analysis

From the mentioned analysis, it was possible to obtain the σ vs. ϵ curves for the uniaxial tests, the $\overline{\sigma}_u$ vs. ΔA_u curve for the biaxial cases, and the τ_{xy} vs. γ for the shear test. All these curves are presented in the original thesis document. The σ vs. ϵ curve, for the uniaxial x direction analysis, is presented in figure 8. Taking this graphic as an example for both tension and compression, four points are studied carefully. The yield points (σ_Y;ϵ_Y) represent the end of linear elastic regime, while the ultimate points (σ_u;ϵ_u) correspond to the maximum values supported by the sheet in non linear elastic regime.

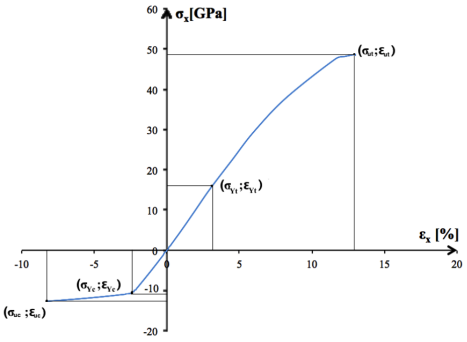

Figure 8: σ vs. ϵ curve for the uniaxial analysis in x direction

From the obtained curves for all the mentioned analyses, the mechanical properties were then calculated, assuming that the thickness of the sheet is $3,20$ [Å] [9]. Using the elasticity equations provided by Beer *et al.* [3], the linear elastic properties were obtained for the yield points. For the non linear elastic regime, the ultimate values were identified using the obtained curves. The calculated results for both regimes are presented in table 2, as well as some results from the literature. Different techniques were used in the literature results, such as MD [1, 9, 24, 25, 26], DFT [2, 21] and FEM [8].

4.2. Discussion of results

In this subsection, the results for the linear and non linear elastic properties presented in table 2 will be discussed and compared with greater focus on the tension cases.

For the linear elastic properties, from the uniaxial tests it is predicted that γ-graphyne exhibits an orthotropic behaviour for both tension and compression cases. The calculated Young modulus for the tension tests were $512,6$ and $507,8$ $[GPa]$ for x and y directions (1% difference), respectively. Most of these results are in good agreement with those presented in literature, especially with the ones that were obtained with MD techniques. For the E_x, the lowest differences between the calculated results and the literature results were $2,4$% with Zhao *et al.*[26], $3,9$% with Cranford and Buehler [9] and $5,5$% with Yang *et al.* [25], while the major verified difference was 14% with Ajori *et al.* [1]. For the E_y, the lowest differences were $0,4$% [1] and $0,9$% [26], while the biggest difference was 37% [9] (this reported result also shows a significant difference regarding the other shown results). For these two properties, the differences were bigger in the reported beam FE model [8] results. This approach is less accurate than the one presented in this work due to the fact that a value for the cross-sectional diameters of the beams has to be assumed or because of the assumption that the bond angle resistance force constant is approximately equal to the bending stiffness of a single beam [12]. For both tested directions, the calculated Poisson coefficients were $> 0,5$, demonstrating huge differences when compared to the literature results. For plane-strain elasticity, the relation between 2D and 3D Poisson coefficient is given by the following equation proposed by Eischen and Torquato [10]:

$$\nu^{(3D)} = \frac{\nu^{(2D)}}{1+\nu^{(2D)}}, \tag{9}$$

where $\nu^{(2D)}$ and $\nu^{(3D)}$ are the 2D and 3D Poisson coefficients, respectively. By using this relation to convert the calculated Poisson coefficients from 2D to 3D, the obtained values for this property are about $0,4$, which is in good agreement with the majority of reported results. For the biaxial tension case, $K_{xy} = 295,1$ $[N/m]$ was obtained. This result shows a small difference $(5,1\%)$ regarding the one obtained by Rouhi *et al.* [24] using MD techniques, while when compared to the DFT reported results by Asadpour *et al.* [2] and Peng *et al.* [21] the differences are approximately 50%. For the shear test, $G_{xy} = 127,1$ $[GPa]$ was calculated, and this result is in good agreement with Zhao *et al.* [26] results, with a $1,2$% difference, while for the DFT [2, 21] reported results, a difference of 80% between shear modulus values is verified.

For the non linear elastic properties, from the uniaxial tests the ultimate stress and extension values $(\sigma_u;\epsilon_u)$ were determined using the σ vs. ϵ curves. By the analysis of these curves, one can conclude that the stiffness of the sheet starts decreasing after the yielding point, for both tension and compression cases. The obtained results for the tension tests were $\sigma_{u,x} = 48,6$ $[GPa]$ and $\epsilon_{u,x} = 13,0$ [%], and $\sigma_{u,y} = 72$ $[GPa]$ and $\epsilon_{u,x} = 16,9$ [%], for the x and y directions, respectively. The bigger values verified for the y direction may be explained considering that there is a greater number of acetylenic groups aligned with the direction of the imposed displacements [9]. These results are in good agreement with the majority of those found in literature. For direction x, the lowest verified differences between the calculated and reported values for the $\sigma_{u,x}$ were $0,8$% [25] and $7,7$% [9], while for direction y the lowest differences were 11% [25] and $18,3$% [21]. For both directions, the differences for the ultimate extension values varied between $10-18$%, while the highest differences for ultimate stress and extension values were approximately 40% [26]. In the non linear elastic regime, the Poisson coefficient decreased with the increase on applied strain. For the biaxial tension test, $\overline{\sigma}_u = 6,6$ $[N/m]$ and $\Delta A_u = 2,4$ [%] were obtained. It was noted that K_{xy} decreases as well in non linear elastic regime. For the shear test, the obtained results demonstrated a linear relationship between the shear stress and angle, so one can conclude that for this test the sheet was not strained enough to reach the non linear elastic regime.

It is noted that for all the uniaxial and biaxial analysis the yielding and ultimate stresses are lower on compression cases, and also occur for lower extension values when compared to the tension ones. From this one can conclude that the Young modulus, Poisson coefficients and bulk moduli calculated for compression cases will be lower than the obtained for tension tests. By comparing them with literature results, one can validate the obtained results and conclude that they are in good agreement with the majority of the literature results. It is

Table 2: Comparison of the present work results and the literature ones

Method	FEM	MD	MD	FEM	DFT	DFT	MD	MD	MD	
Property	Present	[9]	[24]	[8]	[21]	[2]	[25]	[1]	[26]	Units
E_x	164	170,4	140	229,9	-	-	155	-	-	N/m
	(512,6)	(532,5)	-	(718,5)	-	-	-	(586)	(525)	(GPa)
ν_{yx}	0,75	-	-	0,42	-	-	-	0,48	0,17	
$\sigma_{u,x}$	15,6	-	-	-	17,8	-	14,4	-	23,8	N/m
	(48,6)	(48,2)	-	-	-	-	-	(55,6)	-	(GPa)
$\epsilon_{u,x}$	13	8,2	-	-	20	-	11,2	11,7	18	%
E_y	162,5	224	130	209,8	-	-	150	-	-	N/m
	(507,8)	(700)	-	(655,7)	-	-	-	(510)	(503,1)	(GPa)
ν_{xy}	0,73	-	-	0,4	-	-	-	0,64	0,19	
$\sigma_{u,y}$	23	-	-	-	18,8	-	20,47	-	30,8	N/m
	(72)	(107,5)	-	-	-	-	-	(53,7)	-	(GPa)
$\epsilon_{u,y}$	16,9	13,2	-	-	20	-	11,7	13,8	24,7	%
K_{xy}	295,1	-	280	166	-	122,7	-	-	-	N/m
$\overline{\sigma}_u$	6,6	-	-	-	20,6	-	-	-	-	N/m
G_{xy}	40,68	-	-	71	-	77,04	-	-	-	N/m
	(127,1)	-	-	-	-	-	-	-	(128,6)	(GPa)

expectable that some differences may occur when comparing them with the literature results, because the MD and DFT based methods are more efficient and realistic for atomistic simulations (predicting the fracture initiation and propagation). Even so, the presented model shows better agreement with the MD and DFT based studies results when compared to the other reported FE model.

5. Influence of vacancy defects

Different types of defects can occur on the crystalline structure of a nanomaterial and influence its properties. A vacancy defect is known as a defect in which an atom is missing from one of the lattice sites. This section proposes to evaluate the influence of vacancy defects in mechanical properties of γ-graphyne. Ajori *et al.* [1] has already studied the influence of this kind of defects in the mechanical behaviour of γ-graphyne, using an MD simulation on the basis of Tersoff-Brenner potential function. These authors modelled two sheets with 1% of the atoms missing for both mapped and random shapes. They concluded that the vacancy defects reduce Youngs modulus, ultimate stress and strain, and increase Poissons ratio. Moreover it was reported that the vacancy defects in random shapes have a higher effect on these properties than mapped ones.

5.1. Geometric modelling defects

In order to study the influence of vacancy defects in γ-graphyne's structure, three different methodologies were defined to model the defects. For each one, seven different sheets were modelled by increasing the (%) of removed atoms between each one. All three will be described below.

- Vacancy defects in central aromatic rings (a)

Using the perfect γ-graphyne sheet, an aromatic benzenic ring from the central location of a sheet was first removed. The other six sheets were obtained by successively removing one more neighbouring aromatic ring for each one. The (%) of removed atoms varied from $0,57\%$ to $3,28\%$ in the first and seventh sheets modelled with type (a) defects. These two sheets are shown in figures 9 a) and b). Note that the angle bending and vdW springs were visually omitted.

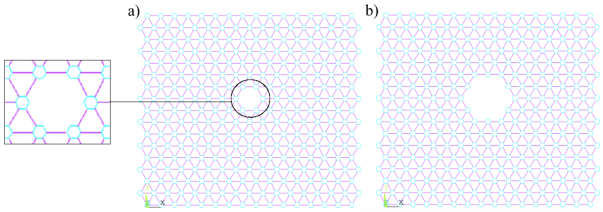

Figure 9: a-b) First and seventh sheets modelled with vacancy defects (a)

- Vacancy defects in dispersed aromatic rings (b)

For the second defined methodology, the purpose was to remove aromatic rings from dispersed locations. The first sheet modelled was the same presented for the type (a) defects. From that one, six more sheets were modelled removing one more dispersed aromatic ring in each one. The (%) of removed atoms varied from $0,57\%$ to $3,98\%$ in the first and seventh sheets modelled with type (b) defects. The second and seventh modelled sheets are presented in figures 10 a) and b), respectively.

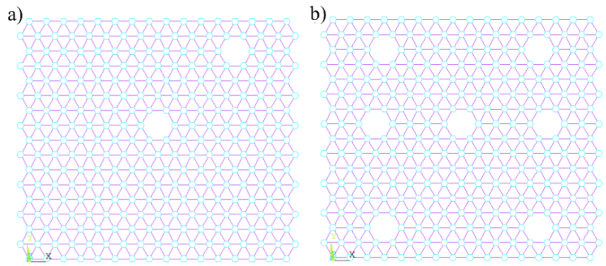

Figure 10: a-b) Second and seventh sheets modelled with vacancy defects (b)

- Vacancy defects in random acetylenic groups (c)

The third methodology consisted in randomly removing acetylenic groups from the perfect γ-graphyne sheet. These defects in similar locations used for the type (b) defects were tried to be applied, removing six more acetylenic groups per each modelled sheet. The (%) of removed atoms varied from $0,38\%$ to $2,34\%$ in the first and seventh sheets modelled with type (c) defects. The mentioned two sheets are illustrated in figures 10 a) and b), respectively.

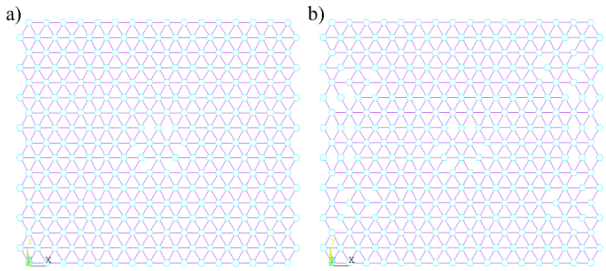

Figure 11: a-b) First and seventh sheets modelled with vacancy defects (c)

5.2. Results presentation

For all the twenty one defective sheets, uniaxial tension and compression analyses were carried out for both x and y directions. From these tests, it was possible to study the influence of these defects on several mechanical properties, by comparing the obtained results with the ones for the perfect sheet. For the linear elastic properties, the Young modulus and the Poisson coefficient were evaluated, while for the non linear elastic ones the ultimate stress and extension values were obtained. All these properties were calculated from the obtained σ vs. ϵ curves, as it was done for the perfect sheet. In figure 12 the x direction corresponding curves for the perfect and type (a) defective sheets is shown.

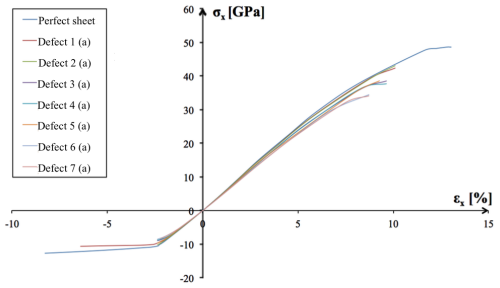

Figure 12: σ vs. ϵ curves for the perfect and type (a) defective sheets

As mentioned before, from all the σ vs. ϵ curves it was possible to calculate the linear and non linear elastic properties for all the defective modelled sheets. All the obtained data are reported in the original thesis document. In order to better understand the influence of simulated defects in E and σ_u values, some graphics were obtained for the variation of $E^{def.}/E^{per.}$ and $\sigma^{def.}/\sigma^{per.}$ ratios per the (%) of removed atoms. The graphics obtained for the direction x tension cases are presented in figures 13 and 14, for the E and σ_u ratios, respectively.

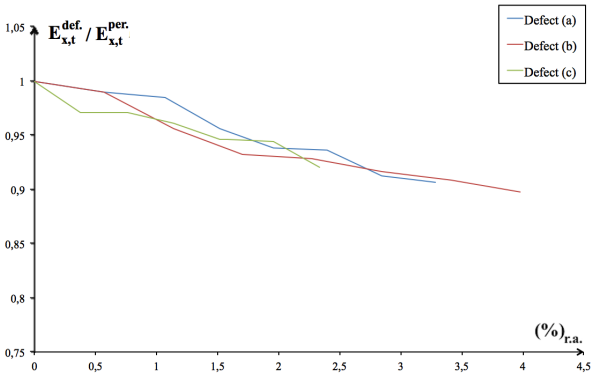

Figure 13: $E^{def.}/E^{per.}$ variation with $(\%)_{r.a.}$ for uniaxial tension test in x direction

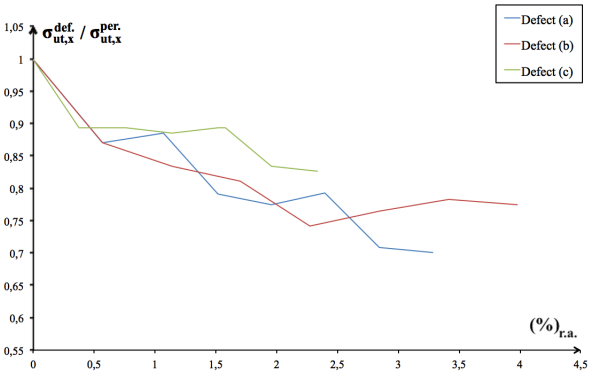

Figure 14: $\sigma^{def.}/\sigma^{per.}$ variation with $(\%)_{r.a.}$ for uniaxial tension test in x direction

5.3. Discussion of results

In this subsection, the obtained results for the defective sheets will be discussed and compared with the ones reported by Ajori *et al.* [1]. For direct tension results comparison, the first sheet with type (a) and (b) defect are compared with the mapped shape sheet presented by Ajori *et al.*, while the fifth sheet with type (c) defect is compared with the random shapes sheet, as illustrated in figures 15 a-d).

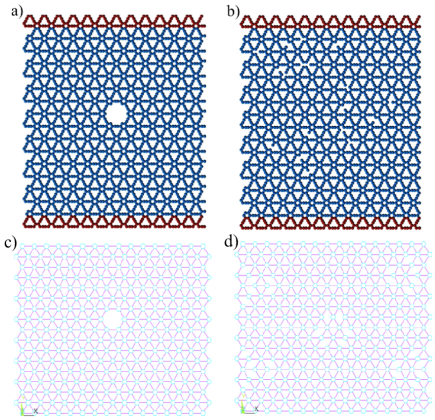

Figure 15: a-b) Ajori *et al.* [1] mapped and random shaped defective sheets; c-d) First and fifth defective modelled sheets for type (a) and (c) defect

For the linear elastic properties, in most cases a decrease in the stiffness of the sheet with the increase of $(\%)_{r.a.}$ was verified, as can been seen in the graphic of figure 13. The comparison between the Young modulus results of the seventh modelled sheet for each type of defects and the perfect one showed that the type (b) defect sheet was the one that exhibits bigger differences in tension and compression tests, decreasing respectively, $10,2\%$ and $19,5\%$ in x direction, and $9,1\%$ and $22,7\%$ in y direction. This may be due to the fact that this sheet has a bigger $(\%)_{r.a.}$ than the other two from type (a) and (c). In the two sheets illustrated in figures 15 a) and b), Ajori *et al.* reported that the Young modulus decreased, in the first one, $7,4\%$ and $5,5\%$ in both x and y directions, respectively, and in the second one, $10,3\%$ and $11,6\%$ for the same directions, respectively. These results suggest that the random effects have bigger impact on the verified loss of the stiffness of the sheet. These results are in good agreement with those obtained for the sheets shown in 15 c) and d). The fifth type (c) defect sheet exhibits a larger decrease in its stiffness, $5,4\%$ and $8,1\%$ for x and y directions, respectively. In the last modelled sheets, the Poisson coefficient decreased between $0,01$-$0,03$ for tension analysis, and $0,05$-$0,12$ for compression tests. Ajori *et al.* reported an increase in the Poisson coefficient, while for the sheets used for comparison, a small decrease was verified as it was reported for all the seventh sheets.

For the non linear elastic regime, the stiffness of the deffective sheets will continue decreasing until the last step of the analysis. Also, the ultimate stresses and strains decreased in the majority of tested cases, with the increase of $(\%)_{r.a.}$, as can be seen in figure 14 for the tension test in x direction. By comparing the difference of results between the last modelled sheets and the perfect sheet, it is noted that the type (a) defect was the one that exhibits bigger differences in the obtained ultimate properties for tension and compression, for both tested directions. From tension tests in x direction, a decreasing of $29,8\%$ and $32,8\%$ for σ_u and ϵ_u was verified respectively, while for the y direction, the differences obtained for these two properties were 50% and $52,7\%$. The results proposed by Ajori *et al.* suggest that the vacancy defects cause a decrease on the ultimate mechanical properties. In the mapped defective sheet, figure 15 a), the authors reported a decreasing in σ_u values of 5% and 23% in the x and y directions, respectively, while in the random defective sheet, figure 15 b), the differences were 21% and 25% for the same directions. By comparing the results calculated for the perfect modelled sheet tension analysis with the ones obtained for the presented sheets in figures 15 c) and d), the σ_u values decreased $13,9\%$ and $29,8\%$ in the type (a) defective sheet in x and y directions, and in the type (c) sheet the values lowered $10,7\%$ and $27,6\%$ for both tested directions, respectively. The ϵ_u calculated values exhibit the same decreasing behaviour verified for σ_u, reported as well by Ajori *et al.*. The obtained results for these two properties were in good agreement with the ones reported by Ajori *et al.*, showing that the random vacancy defects induced a bigger decrease on the ultimate stresses and strains of the sheets.

From the obtained results for both linear and non linear elastic properties, one can conclude that the vacancy defects in the majority of tested cases lead to a decrease on mechanical properties of γ-graphyne. In general, the defects located in the centre of the sheets showed smaller differences when compared to the perfect ones. This may be due to the fact that the defects of these sheets are not located next to the zones influenced by boundary conditions, as verified for the type (b) and (c) defective ones. Also, the presence of defects in multiple locations of the sheet makes it weaker in different regions, so these sheets are more likely to have a major influence on its properties caused by the vacancy defects. Specifically speaking about the compression cases, the obtained results exhibit bigger differences when compared to the calculated results for tension tests. It was noted that there is an in-

crease in the values of the linear and non linear elastic properties when the $(\%)_{r.a.}$ increases, as can be seen in the graphics of figures 13 and 14. These exceptions were verified for both tension and compression tests. This may be due to the fact that some of the defective modelled sheets exhibit an axisymmetric structure, which has a direct influence under the mechanical properties of the sheets. These increased values occurred more significantly in the compression tests, due to the fact that the sheets exhibit less stiffness in these cases and there are highly deformed zones on locations near the applied boundary conditions. Also the potentials used in the presented model cannot predict the electronic repulsive forces that are present on a molecular structure when the atoms get closer. The differences reported between the presented and the Ajori *et al.* [1] results are expectable because different approaches were used. Even so, the overall obtained results exhibit good agreement with the literature ones.

6. Conclusions

This article was an extended summary of the thesis that was set out to characterize the nonlinear mechanical properties of perfect and imperfect γ-graphyne sheets. The presented model agrees with the literature results, proving that it can be used to estimate good approximations of these properties in a faster way when compared to MD and DFT techniques.

The main conclusions of this thesis are summarized in this paragraph. The developed model for the perfect γ-graphyne sheet demonstrates good precision in determining the linear and non linear elastic properties. The obtained results exhibit agreement with the literature reported ones, provided by more complex techniques. The choice of spring FEs instead of beam FEs had a direct impact on the proximity between the presented model and the MD and DFT based ones. Also, the proposed model demonstrated to be a good approach to study the influence of vacancy defects in mechanical properties of γ-graphyne. It was concluded that an increase on the percentage of removed atoms causes, in the majority of tested cases, a decrease on these properties. Also, the distribution of defects (mapped or random) showed different decreasing results for the evaluated properties. The defects located near the applied boundary conditions induce a greater decrease on the mechanical properties of γ-graphyne.

From the work presented in this thesis, it is believed that there are some developments that can be made. Some examples are:

- Parametrize the dimensions of the γ-graphyne sheets and evaluate the dependence of the mechanical properties on the sheet dimension.
- Study the influence of vacancy defects in the bulk modulus and the shear modulus.
- Include fracture prediction models in order to study the initiation and propagation of fractures in the structure of γ-graphyne.

Acknowledgements

First of all, I would like to thank my supervisor, Professor Nuno Silvestre, for my motivation and confidence while working under his supervision, and for the guidance and patience he has shown me since the beginning of my work.

Also, I'm greatful to my family, my girlfriend and my close friends. They provided me all the love and necessary conditions to accomplish this objective.

Finally, I would like to express my gratitude to Instituto Superior Técnico and all the professors with whom I have studied, for helping me grow both intellectually and as a person.

References

[1] S. Ajori, R. Ansari, and M. Mirnezhad. Mechanical properties of defective gamma-graphyne using molecular dynamics simulations. *Materials Science and Engineering A*, 561:274–289, 2013.

[2] M. Asadpour, S. Malakpour, M. Faghihnasiri, and B. Taghipour. Mechanical properties of two-dimensional graphyne sheet, analogous system of BN sheet and graphyne-like BN sheet. *Solid State Communications*, 212:46–52, 2015.

[3] F. P. Beer, E. R. Johnston Jr., and J. T. DeWolf. *Mechanics of Materials*. McGraw Hill Higher Education, 4th edition, 2005.

[4] S. Bellucci, C. Balasubramanian, F. Micciulla, and G. Rinaldi. CNT composites for aerospace applications. *Journal of Experimental Nanoscience*, 2:193–206, 2007.

[5] T. Belytschko, S. P. Xiao, G. C. Schatz, and R. Ruoff. Atomistic Simulations of Nanotube Fracture. *Physical Review B*, 65, 2002.

[6] S. J. Blanksby and G. B. Ellison. Bond Dissociation E. of Organic Molecules. *Acc. Chem. Res.*, 4:255–263, 2003.

[7] C. Cha, S. Shin, N. Annabi, M. Dokmeci, and A. Khademhosseini. Carbon-based nanomaterials: Multifunctional materials for biomedical engineering. *ACS Nano*, 7:2891–2897, 2013.

[8] R. Couto and N. Silvestre. Finite Element Modelling and Mechanical Characterization of

Graphyne. *Journal of Nanomaterials*, 2016:1–15, 2016.

[9] S. W. Cranford and M. J. Buehler. Mechanical properties of graphyne. *Carbon*, 49:4111–4121, 2011.

[10] J. W. Eischen and S. Torquato. Determining elastic behavior of composites by the boundary element method. *J. Appl. Phys.*, 159, 1993.

[11] S. Georgantzinos, D. Katsareas, and N. Anifantis. Graphene characterization: A fully non-linear spring-based finite element prediction. *Physica E: Low-Dimensional Systems and Nanostructures*, 43:18331839, 2011.

[12] G. I. Giannopoulos, P. A. Kakavas, and N. K. Anifantis. Evaluation of the effective mechanical properties of SWCNT using a spring based finite element approach. *Computational Materials Science*, 41:561–569, 2008.

[13] M. M. Haley. Synthesis and properties of annulenic subunits of graphyne and graphdiyne nanoarchitectures. *Pure and Applied Chemistry*, 80:519–532, 2008.

[14] M. I. Katsnelson. Graphene: carbon in two dimensions. *Materials Today*, 10:20–27, 2007.

[15] T. Kukowski. Lightweight cnt cables for aerospace. ESC NDE technology assessment NASA NDI workshop, Johnson Space Center Houston, TX, 2012.

[16] J. Lennard-Jones. From the Variation of the Viscosity of a Gas with Temperature. *Proceedings of the Royal Society of London. Series A*, 1924.

[17] P. M. Morse. Diatomic molecules according to the wave mechanics. II. Vibrational levels. In *Physical Review*, volume 34, pages 57–64. 1929.

[18] G. M. Odegard, T. S. Gates, L. M. Nicholson, and K. E. Wise. Equivalent-continuum modeling of nano-structured materials. *Composites Science and Technology*, 62:1869–1880, 2002.

[19] G. M. Odegard, T. S. Gates, K. E. Wise, C. Park, and E. J. Siochi. Constitutive modeling of nanotube-reinforced polymer composites. *Composites Science and Technology*, 63:1671–1687, 2003.

[20] Q. Peng, A. K. Dearden, J. Crean, C. Liang, H. Sheng, and S. De. New materials graphyne, graphdiyne, graphone, and graphane: review of properties, synthesis, and application in nanotechnology. *Nanotechnology, Science and Applications*, 7:1–29, 2014.

[21] Q. Peng, W. Ji, and S. De. Mechanical properties of graphyne monolayers: a first-principles study. *Physical Chemistry Chemical Physics*, 14:13385–13391, 2012.

[22] S. Pezzin, L. Coelho, and S. Amico. New generation of multifunctional composites with carbon nanotubes for space applications. *Polymers in Defence and Aerospace Applications*, 2010.

[23] R. Rafiee and M. Heidarhaei. Investigation of chirality and diameter effects on the Young's modulus of carbon nanotubes using non-linear potentials. *Composite Structures*, 94:2460–2464, 2012.

[24] S. Rouhi, T. Pour Reza, B. Ramzani, and S. Mehran. Investigation of the vibration and buckling of graphynes: A molecular dynamics-based finite element model. *Proceedings of the Institution of Mechanical Engineers, Part C: Journal of Mechanical Engineering Science*, 0:96–132, 2016.

[25] Y. Yang and X. Xu. Mechanical properties of graphyne and its family - A molecular dynamics investigation. *Computational Materials Science*, 61:83–88, 2012.

[26] J. Zhao, N. Wei, Z. Fan, L. Liang, and T. Rabczuk. The mechanical properties of three types of carbon allotropes. *Nanotechnology*, 24, 2013.